

Multimodal brain tumor classification

Marvin Lrousseau^{1,2}, Eric Deutsh¹, and Nikos Paragios³

¹ Paris-Saclay University, Gustave Roussy, Inserm, 94800, Villejuif, France

² Paris-Saclay University, CentraleSuplec, 91190, Gif-sur-Yvette, France

³ TheraPanacea, 75014, Paris, France

Abstract. Cancer is a complex disease that provides various types of information depending on the scale of observation. While most tumor diagnostics are performed by observing histopathological slides, radiology images should yield additional knowledge towards the efficacy of cancer diagnostics. This work investigates a deep learning method combining whole slide images and magnetic resonance images to classify tumors. Experiments are prospectively conducted on the 2020 Computational Precision Medicine challenge, in a 3-classes unbalanced classification task. We report cross-validation (resp. validation) balanced-accuracy, kappa and f1 of 0.913, 0.897 and 0.951 (resp. 0.91, 0.90 and 0.94). The complete code of the method is open-source at ‡⁴, and as a Dockerfile at †. Those include histopathological data pre-processing, and can therefore be used off-the-shelf for other histopathological and/or radiological classification.

Keywords: Histopathological classification · Radiology classification · Multi-modal classification · Tumor classification · CPM RadPath.

1 Introduction

Gliomas are the most common malignant primary brain tumor. They start in the glia, which are non-neuronal cells from the central system that provide supportive functions to neurons. There are three types of glia, yielding different types of brain tumor: astrocytomas develop from astrocytes, tumors starting in oligodendrocytes lead to oligodendrogliomas, and ependymomas develop from ependymal cells. The most malignant form of brain tumors is glioblastoma multiforme, which are grade IV astrocytomas. Additionally, some brain tumor may arise from multiple type of glial cells, such mixed gliomas, also called oligo-astrocytomas.

In the clinical setting, the choice of therapies is highly influenced by the tumor grade [15]. In such context, glioblastoma are grade IV, astrocytoma are grade II or III and oligodendroglioma are grade II. With modern pushes towards precision medicine, a finer characterization of the disease is considered for treatment strategies. Such therapeutic strategies can be surgery, radiation therapy, chemotherapy, brachytherapy or their combinations such as surgery followed by neo-adjuvant radiation therapy. Historically, the classification of brain

⁴ ‡: will be communicated in a modified version of this paper upon challenge ending

tumors has relied on histopathological inspection, primarily characterized with light-microscopy observation of H&E-stained sections, as well as immunohistochemistry testing. This histological predominance have been contrasted with the recent progress in understanding the genetic changes of tumor development of the central nervous system. Additionally, while it is not used in neoplasm diagnostic, neuro-imaging can bring other information regarding the state of the disease.

This work deals with a novel strategy for classifying tumors with several image types. We present a strategy to classify whole slide images and/or radiology images extracted from a common neoplasm. Experiments are conducted on a dataset made of pairs of histopathological images and MRIs, for a 3-categories classification of brain tumor.

1.1 Related work

Whole slide image classification Whole slide images (WSI) are often at gigapixel size, which drastically impede their processing with common computer vision strategies. By essence, a WSI is obtained at a certain zoom (called magnification), from which lower magnifications can be interpolated. Therefore a first strategy for WSI classification would consist in downsampling a full-magnification image sufficiently to be processed by common strategies. However, since the constituent elements of WSIs are the biological cells, downsampling should be limited or the loss of information could completely prevent the feasibility of the task.

One first strategy therefore consists in first classification tiles extracted from a WSI, which is equivalent to WSI segmentation, and then combine those tile predictions into a slide prediction. This was investigated for classifying glioma in [7], breast cancer in [4], lung carcinoma in [2], and prostate cancer, basal cell carcinoma, and breast cancer metastases to axillary lymph nodes in [1]. More generally, the segmentation part of these works has been unified in [14]. For combining tile predictions into slide predictions, numerous strategies exist such as ensembling or many other technics that fall under the umbrella of instance-based multiple instance learning [3].

One limitation with such decoupled approach is that the tile classifier method does not learn useful features to embed tiles into a latent space which could be sampled by a slide classification method. A generalization consists in having a first model that converts tiles into an embedded (or latent) vector, and a second model which combines multiples such vectors from multiple tiles into a single WSI prediction. This is known as embedded-based multiple instance learning [3]. The function that maps the instance space to the slide space can be max-pooling, average-pooling, or more sophisticated functions such as noisy-or [20], noisy-and [12], log-sum-exponential [16], or attention-based [9].

Brain tumor classification with MRIs There are two major approaches for MRI classification. The first is called radiomics [13], and consists in first extracting a set of features for all images of a training set. Such features typically

consist in clinical features such as age, first-order features such as descriptors of tumor shape or volume, and second order features describing textural properties of a neoplasm. These features are then used by common machine learning algorithms as a surrogate of crude MRIs. Examples of such approaches for brain tumor classification are illustrated in [21] and [11]. The major limitation of radiomics lies in the fact that tumor volumes must be annotated beforehand in order to extract meaningful features.

The other general approach of tumor classification from MRIs consists in using end-to-end deep learning systems. Deep learning bypasses the necessity of delineating the tumor volume, and is more flexible than traditional machine learning since features are learned on-the-fly. Compared to machine learning methods, deep learning is known to require more training samples, but outcompetes the former when the number of data is sufficient. The majority of variability of brain tumor classification studies relying on deep learning lies in the architecture used. Examples of such studies are [17] or others identified in [19].

2 Methods

Our proposed method leverages both imaging and histological modalities through an ensemble. Specifically, a first deep learning model is intended to classify WSIs, while a second network classifies MRIs.

2.1 Whole slide image classification

Our WSI classifier bears most concepts in multiple instance learning approaches as depicted in Fig.1. At training and inference, a WSI is split into non-overlapping tiles. Each tile is forwarded into a standard 2D image classifier, such as a ResNet [6] or an EfficientNet [18], whose classifier layer has been removed. Each tiled is thus embedded into a latent vector of size L . For a bag of n tiles, a latent matrix of size $n \times L$ is obtained. Then, a max-pooling operation is performed on each feature - that is, across the n dimension. Similarly, average pooling is performed for each feature. Both max-pooled and average-pooled are concatenated, making a resulting vector of size $L + L = 2L$. Finally, a classifier network ("head") processes this pooled latent vector into a 1 class prediction. This head is made of a dropout layer, followed by a final classification layer with softmax activation.

This system can be implemented end-to-end in a single network, for standard deep learning optimization. The head part can be more sophisticated, with the addition of an extra linear layer, followed by an activation function such as ReLu, and batch normalization. This implementation was kept simple due to the low number of training samples in our experiments. Of major interest, the slide embedding output of size $2L$ is independent of the size n of the input bag. Consequently, bags of any size can be fed into the network during training or inference.

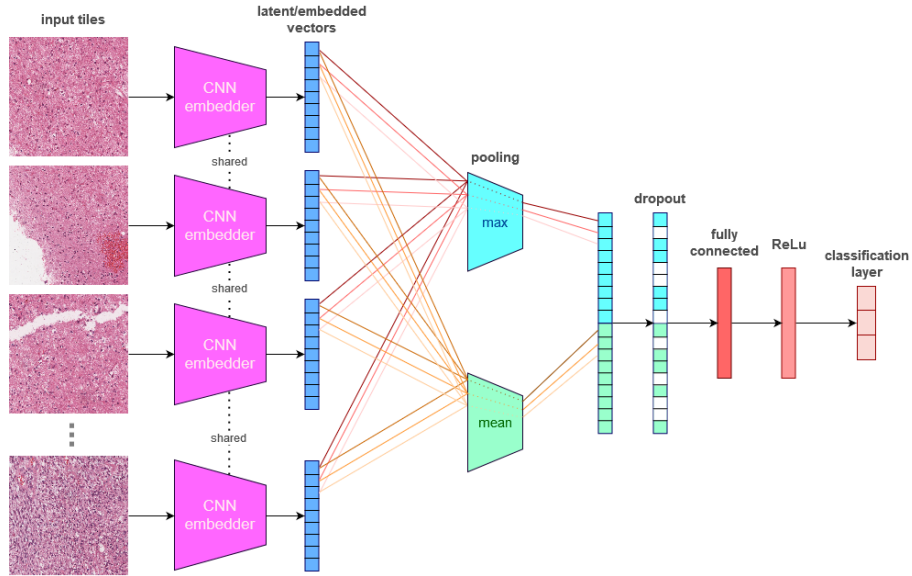


Fig. 1: Schematic representation of the end-to-end WSI classification strategy. A set of tiles is extracted from a WSI, and are each inferred into a unique learnable CNN embedder (i.e. CNN classifier whose last layer has been discarded). Each of the tiles is thus converted into a latent vector (blue vectors) of size L , where $L = 9$ in this figure. Each latent dimension is then maxed, and simultaneously averaged, into two vectors of size L , which are then concatenated into a vector of size $2L$. This WSI latent vector is then forwarded into a dropout and a finale classification layer.

During inference, it is common that the number of non-overlapping tiles is above the memory limit induced by the network, which is roughly the memory footprint of the embedding model. For instance, the number of tiles per slide is depicted in Fig. 3 for the training samples at magnification 20. Typically, for EfficientNet_b0 embedding model, only 200 tiles can be fitted in a 16Gb graphic card. Therefore, during inference, a random set of tiles is sampled from a WSI, each yielding one predicted class. The resulting finale predicted class is obtained by hard-voting the latter.

2.2 Medical imaging resonance classification

Our MRI classification pipeline is straightforward and consists in a single network direct classification of the 4D volumes made of all 4 modalities. Specifically, we use a Densenet [8] made of 164 layers. The Densenet family was used due to its low number of parameters, which seems appropriate to the low number of experiment training samples, and its dense number of residual connections which alleviate much gradient issues. To accommodate with the 3D spatial dimensions

of input volumes, the 2D convolutions, and the pooling operators have been modified to 3D.

2.3 Multi-modal classification through ensembling

Ensembling was performed for multiple reasons. First of all, without any a priori, histopathological classification could detect different features at various scales, thus producing different or complementary diagnostics depending on the input magnification. In our implementation, multiple networks were trained at various magnifications. Secondly, ensembling allow to use both histopathological and radiological modalities to determine a final diagnostic. Finally, ensembling a number of neural networks is known to significantly improve the performance and robustness of a neural network system [5]. For these reasons, our final classification uses an ensemble of multiple histopathological networks, radiological networks in a soft-voting way. Besides, as shown in [22], it may be advantageous to ensemble some of the at-hand neural networks rather than all of them. As discussed in 3.2, a portion of the trained networks is discarded in the finale decision system.

3 Experiments

Experiments were conducted during the 2020 Computational Precision Medicine Radiology-Pathology challenge (CPM-RadPath 2020). All the data is provided by the organizers, i.e. a training set and an online validation set. Additionally, final results are computed on a hidden testing set with only one try, such as to minimize testing fitting. Our team name was *marvinler*.

3.1 Data

Dataset The training data consists in 221 cases extracted from two cohorts: The Cancer Image Archive (TCIA) and the Center for Biomedical Image Computing and Analytics (CBICA). For each case, one formalin-fixed, paraffin-embedded (FFPE) resection whole slide image was provided, along with one MRI, which consists in 4 modalities: T1 (spin-lattice relaxation), T1-contrasted, T2 (spin-spin relaxation), and fluid attenuation inversion recovery (FLAIR) pulse sequences.

Each case belongs to one of three diagnostic categories among astrocytomas, oligodendrogliomas, and glioblastoma multiforme. This information was provided for each training case. On top of that, a similar validation set made of 35 cases was available for generalization assessment. For these cases, ground-truth labels were hidden, although up to 50 submissions were possible, with feedback containing balanced accuracy, f1 score, and kappa score. Fig. 2 shows an example of validation sample (CPM19_CBICA_AAK_1).

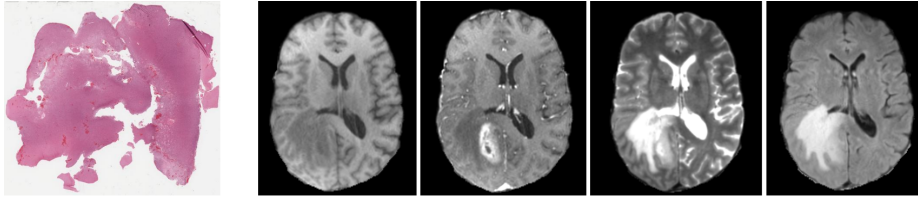


Fig. 2: Example of data point from the online validation set. The image on the left is a downsampled version of the whole slide image which is initially of width 96224 pixels and of height 82459 pixels. The four images on the right represent the MRI of the same case, and are, by order, the T1, the T1 contrast-enhanced, the T2, and the FLAIR modalities. For the MRI, the same slice extracted from each 3D volume is represented. Each 3D volume is initially of size 240x240x154 pixels.

Pre-processing No data pre-processing were performed on MRIs. Indeed, those images have already been skull-stripped, and bias-field corrected. Other MRI processing were subcontracted to the radiology data augmentation step, as detailed in 3.2.

Whole slide images were available in non-pyramidal .tiff format. They were first tiled in a pyramidal scheme using libvips, with a tile width of 512 pixel and no tile overlap. For each resulting magnification level, all tiles considered background were discarded. This was done by detecting tiles where at least 75% of pixels have both red, green, and blue channels above a value of 180 (where 255 is absolute white and 0 is black), which saved more than two third of disk space by discarding non informative tile from further processing. After this filtering, the number of tiles per slide is depicted in the histogram of Fig. 3 for magnification 20. The complete WSI pre-processing was applied to both training, validation, and testing sets.

3.2 Implementation details

A pre-trained Efficientnet_b0 was selected as the histopathological model embedder, converting 224 pixel-wide images into an embedded vector of size $L = 1280$. During training, 50 tiles were selected from 4 WSIs, resulting in a batch of size 200. Each tile was data augmented with random crop from 512 pixel width to 224 pixel width, color jitter with brightness, contrast, saturation of 0.1, and hue of 0.01, and was normalized by dividing the mean and standard deviation of each RGB channel as computed on the training dataset. To counter the low number of training samples, dropout of 0.5 was used in the head of the network. The final softmax activation was discarded during training, and cross entropy loss was used to compute the error signal (which contains a log softmax operation for numerical stability). To handle class imbalance, weights were computed as the inverse of the frequency of each of the 3 classes, and used in the error computation. Adam [10] optimizer was used to back-propagate the error signal, with

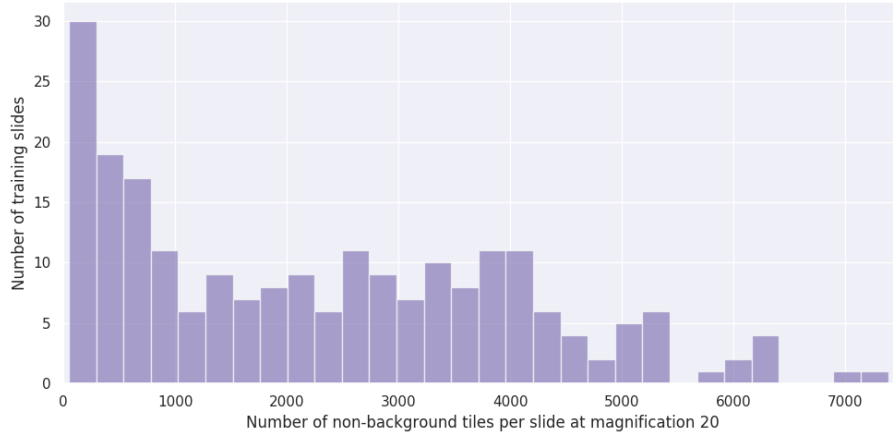


Fig. 3: Histogram of the number of tiles considered non-background for all training slides at magnification 20, or equivalently micrometer per pixel (mpp) of 0.5.

default momentum parameters and learning rate of $5e - 5$ for 50 epochs. This process was applied for the 4 magnifications of 40, 20, 10, and 5, or equivalently and respectively of micrometer per pixel of 0.25, 0.5, 1, and 2.

For the classification from MRIs, data augmentation first consisted of cropping the foreground, which roughly crops the MRI to their contained brain. These cropped volumes were resized to a unique size of $128 \times 128 \times 128$, and each modality was standard scaled such that 0 values (corresponding to background) were not computed in mean and standard deviation computations. Then, a random zoom between 0.8 and 1.2 was applied, followed by a random rotation of 10 degrees in both sides for all dimensions. Random elastic deformations with parameter values of sigma 10 and magnitude of 200. All of the data augmentation was implemented using the Medical Open Network for AI (MONAI) toolkit⁵, which is also the source of the Densenet164 architecture implementation. Error signal was computed with cross-entropy loss and back-propagated with Adam optimizer for 200 epochs at learning rate $5e - 4$. The same class imbalance was used than the histopathological networks.

For both 5 models (4 histopathological and 1 radiological), the last epoch weights snapshot, as well as the snapshot from the 10 epochs to the end were collected. Following [22], 2 least performing (on the local validation) out of the 10 networks were discarding, which consisted in one radiology-based model and one model from magnification 5. Soft-voting was performed on the 8 resulting models for all slides, and the class with highest probability was assigned as the predicted class.

⁵ <https://github.com/Project-MONAI/MONAI>

3.3 Results

After 3 online submissions, the hidden validation performance was a balanced accuracy of 0.911, a kappa score of 0.904, and an f1 score (with micro average) of 0.943 which ranked us second overall. Unseen testing results are still awaiting. Our cross-validation results are similar, with a balanced accuracy of 0.913, a kappa score of 0.897 and an f1 score of 0.951, denoting a certain high generalization capacity from our approach.

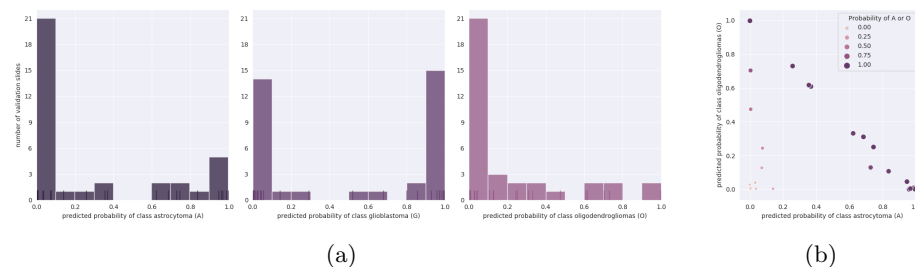


Fig. 4: Analysis of validation predicted probabilities. (a) Histogram of predicted probabilities for all 35 validation cases. Each plot (3 in total) refers to one of the 3 predicted class, as indicating in the x-axis label. (b) Scatterplot of predictions of astrocytoma vs oligodendrogliomas. Color and size of points are proportional to the sum of predictions of the latter class, or equivalently inversely proportional to the predicted probability of glioblastoma multiforme.

For each diagnostic category, a histogram of validation predicted probabilities was computed, resulting in 3 plots depicted in Fig. 4a. Notably, there seems to be less hesitation for the prediction of the glioblastoma multiforme class (G), where only 3 cases were predicted with a probability between 0.2 and 0.8. In comparison, 7 (resp. 9) cases are predicted with a probability between 0.2 and 0.8 for the astrocytoma (A) (resp. oligodendrogliomas (O)). Fig. 4b further highlights that most hesitation comes from both classes A and O, with all probabilities of class A that are not below 0.2 or above 0.8 predicted mostly as class O compared to G. Besides, 6 out of 9 unsure probabilities for the O class were split with the A class compared to the G one. This could illustrate that some cases seem to exhibit both oligodendrogliomas and astrocytoma, known as mixed gliomas. Notably, while mixed gliomas are a valid diagnostic in clinical setting, this class was absent in the challenge data, with a decision between class A and O taken by the challenge annotators for such cases.

4 Conclusion & Discussion

Our work illustrates the feasibility of the classification of tumor types among 3 pre-defined categories. Although testing results are still pending, the proposed

approach appears to generalize well to unseen data from the same distribution. The proposed pipeline heavily relies on histopathological slides, which have been the golden standard for tumor diagnostic for a hundred years. This system is an end-to-end trainable decision system, that rely on a learnable embedding model (e.g. a convolutional neural network) and combine a set of any size of tiles embedded vectors into a slide latent vector for further classification. This generic deep learning pipeline can be taken off-the-shelf and applied to many other histopathological classification tasks, would it be grading, diagnostic, primary determination or prognosis purposes. For this reason, we open-source our complete whole slide image classification method at ‡, including full data pre-processing from WSIs, in order to help reduce the barrier of entry of whole slide image classification.

While our use of the radiology modality has not been heavily in this work, there should be improvement in classifying cases with more information that in a histopathological context. We believe that, with more training data, diagnostic could be further improved with multi-modal solutions that embed both radio images and histo images into a common latent space.

References

1. Campanella, G., Hanna, M.G., Geneslaw, L., Mirafior, A., Silva, V.W.K., Busam, K.J., Brogi, E., Reuter, V.E., Klimstra, D.S., Fuchs, T.J.: Clinical-grade computational pathology using weakly supervised deep learning on whole slide images. *Nature medicine* **25**(8), 1301–1309 (2019)
2. Coudray, N., Ocampo, P.S., Sakellaropoulos, T., Narula, N., Snuderl, M., Fenyö, D., Moreira, A.L., Razavian, N., Tsirigos, A.: Classification and mutation prediction from non-small cell lung cancer histopathology images using deep learning. *Nature medicine* **24**(10), 1559–1567 (2018)
3. Dietterich, T.G., Lathrop, R.H., Lozano-Pérez, T.: Solving the multiple instance problem with axis-parallel rectangles. *Artificial intelligence* **89**(1-2), 31–71 (1997)
4. Gecer, B., Aksoy, S., Mercan, E., Shapiro, L.G., Weaver, D.L., Elmore, J.G.: Detection and classification of cancer in whole slide breast histopathology images using deep convolutional networks. *Pattern recognition* **84**, 345–356 (2018)
5. Hansen, L.K., Salamon, P.: Neural network ensembles. *IEEE transactions on pattern analysis and machine intelligence* **12**(10), 993–1001 (1990)
6. He, K., Zhang, X., Ren, S., Sun, J.: Identity mappings in deep residual networks. In: *European conference on computer vision*. pp. 630–645. Springer (2016)
7. Hou, L., Samaras, D., Kurc, T.M., Gao, Y., Davis, J.E., Saltz, J.H.: Patch-based convolutional neural network for whole slide tissue image classification. In: *Proceedings of the IEEE conference on computer vision and pattern recognition*. pp. 2424–2433 (2016)
8. Huang, G., Liu, Z., Van Der Maaten, L., Weinberger, K.Q.: Densely connected convolutional networks. In: *Proceedings of the IEEE conference on computer vision and pattern recognition*. pp. 4700–4708 (2017)
9. Ilse, M., Tomczak, J.M., Welling, M.: Attention-based deep multiple instance learning. *arXiv preprint arXiv:1802.04712* (2018)
10. Kingma, D.P., Ba, J.: Adam: A method for stochastic optimization. *arXiv preprint arXiv:1412.6980* (2014)

11. Kotrotsou, A., Zinn, P.O., Colen, R.R.: Radiomics in brain tumors: an emerging technique for characterization of tumor environment. *Magnetic Resonance Imaging Clinics* **24**(4), 719–729 (2016)
12. Kraus, O.Z., Ba, J.L., Frey, B.J.: Classifying and segmenting microscopy images with deep multiple instance learning. *Bioinformatics* **32**(12), i52–i59 (2016)
13. Lambin, P., Rios-Velazquez, E., Leijenaar, R., Carvalho, S., Van Stiphout, R.G., Granton, P., Zegers, C.M., Gillies, R., Boellard, R., Dekker, A., et al.: Radiomics: extracting more information from medical images using advanced feature analysis. *European journal of cancer* **48**(4), 441–446 (2012)
14. Lerousseau, M., Vakalopoulou, M., Classe, M., Adam, J., Battistella, E., Carré, A., Estienne, T., Henry, T., Deutsch, E., Paragios, N.: Weakly supervised multiple instance learning histopathological tumor segmentation. *arXiv preprint arXiv:2004.05024* (2020)
15. Louis, D.N., Perry, A., Reifenberger, G., Von Deimling, A., Figarella-Branger, D., Cavenee, W.K., Ohgaki, H., Wiestler, O.D., Kleihues, P., Ellison, D.W.: The 2016 world health organization classification of tumors of the central nervous system: a summary. *Acta neuropathologica* **131**(6), 803–820 (2016)
16. Ramon, J., De Raedt, L.: Multi instance neural networks. In: *Proceedings of the ICML-2000 workshop on attribute-value and relational learning*. pp. 53–60 (2000)
17. Talo, M., Baloglu, U.B., Yildirim, Ö., Acharya, U.R.: Application of deep transfer learning for automated brain abnormality classification using mr images. *Cognitive Systems Research* **54**, 176–188 (2019)
18. Tan, M., Le, Q.V.: Efficientnet: Rethinking model scaling for convolutional neural networks. *arXiv preprint arXiv:1905.11946* (2019)
19. Tandel, G.S., Biswas, M., Kakde, O.G., Tiwari, A., Suri, H.S., Turk, M., Laird, J.R., Asare, C.K., Ankrah, A.A., Khanna, N., et al.: A review on a deep learning perspective in brain cancer classification. *Cancers* **11**(1), 111 (2019)
20. Zhang, C., Platt, J.C., Viola, P.A.: Multiple instance boosting for object detection. In: *Advances in neural information processing systems*. pp. 1417–1424 (2006)
21. Zhou, M., Scott, J., Chaudhury, B., Hall, L., Goldgof, D., Yeom, K.W., Iv, M., Ou, Y., Kalpathy-Cramer, J., Napel, S., et al.: Radiomics in brain tumor: image assessment, quantitative feature descriptors, and machine-learning approaches. *American Journal of Neuroradiology* **39**(2), 208–216 (2018)
22. Zhou, Z.H., Wu, J., Tang, W.: Ensembling neural networks: many could be better than all. *Artificial intelligence* **137**(1-2), 239–263 (2002)